# Structure and Doping Determined Thermoelectric Properties of $Bi_2Se_3$ Thin Films Deposited by Vapour–Solid Technique

Jana Andzane, Krisjanis Buks, Malvine Nelda Strakova, Martins Zubkins, Mikhael Bechelany, Mikelis Marnauza, Margarita Baitimirova, and Donats Erts

***Abstract*—In this work, a simple catalyst-free vapour-solid deposition method was applied for controlled deposition of two types (planar and disordered) of continuous $Bi_2Se_3$ nanostructured thin films on different (fused quartz/glass, mica, graphene) substrates. Characterisation of electron transport (type, concentration and mobility of the main charge carriers) and thermoelectric properties (Seebeck coefficient and power factor) showed that proposed in this work deposition method allows to obtain $Bi_2Se_3$ thin films with power factor comparable and even higher than reported for the $Bi_2Se_3$ thin films grown by molecular beam epitaxy technique. Power factor of the best obtained thin films can be significantly improved by introduction Sb or Fe dopants in low concentrations.**

***Index Terms*—Bismuth selenide, thin film, thermoelectrics, physical vapour deposition, nanostructuring, doping.**

## I. Introduction

THERMOELECTRIC (TE) heat-to-electricity conversion devices are very attractive solution for waste heat capturing and increase of energetical efficiency of variety of industrial and domestic processes. However, the wide commercial application of TE devices is hampered by their low efficiency.

The main strategies for increase of the thermoelectrical (TE) efficiency of materials include the use of numerous interfaces for efficient phonon scattering resulting in reduction of the lattice thermal conductivity, and the use of quantum confinement phenomena to increase the Seebeck coefficient of the material.

Bismuth selenide ($Bi_2Se_3$) is a narrow band gap semiconductor with excellent thermoelectric (TE) properties at near-room temperatures, also representing a new class of materials known as topological insulators. For such materials, quantum confinement introduced by the downsizing down to nanoscale was proposed an efficient method for simultaneous suppression of the thermal conductivity and enhancing of thermoelectrical power factor [1], [2]. The additional method of improvement of the thermoelectric properties of bismuth chalcogenides is specific doping. For example, doping with Sb allows to control charge carrier type and concentration in $Bi_2Se_3$, and position of the Fermi level [3], [4]. Alternatively, doping with Sn or Fe introduces resonant impurity levels (RL) in the electronic structure of bismuth chalcogenides close to Fermi level. This may result in significant improvement of thermoelectric properties of these materials [5]–[7].

For practical applications, catalyst-free vapour-solid deposition of bismuth chalcogenide thin films is favourable due to its simplicity and cost-efficiency. For this method, different substrates like Si, glass, mica [8], indium tin oxide covered glass [9] and graphene [10] has been used. However, the drawback of this method in comparison with molecular beam epitaxy (MBE) deposition technique is lower quality of the deposited thin films.

In this work, the catalyst-free vapour-solid deposition technique [11] was applied for controlled obtaining of two types of continuous nanostructured $Bi_2Se_3$ thin films on different substrates (fused quartz/glass, mica and chemical vapour deposition (CVD) graphene). Planar thin films, consisting of coalesced nanoplates planar to the substrate surface, are suitable for both in-plane and through-plane measurements and layered devices. In turn, disordered thin films, consisting of both planar and randomly oriented relative to the substrate surface nanoplates, have been reported useful for sandwich-type devices [12], as well as are more suitable for sensor applications due to high surface-to-volume ratio. The best of the obtained $Bi_2Se_3$ thin films were doped with antimony (Sb), tin (Sn) and iron (Fe) in different concentrations for further potential improvement of their thermoelectrical efficiency. Structure, electron transport and thermoelectric properties of the deposited thin films were determined and discussed.

## II. Experimental

### A. Deposition of the Thin Films

Nanostructured $Bi_2Se_3$ thin films were deposited by previously reported catalyst-free vapour-solid deposition method using quartz tube furnace (GCL-1100X, MTI Corp) [10]. Evaporation temperature of the source material was 585 °C. Deposition

Manuscript received June 24, 2019; accepted September 1, 2019. Date of publication September 12, 2019; date of current version September 23, 2019. This work was supported by the ERDF projects 1.1.1.1/16/A/257 and 1.1.1.2/1/16/037. The review of this paper was arranged by Associate Editor T.-L. Ren. *(Corresponding author: Jana Andzane.)*

J. Andzane, K. Buks, M. N. Strakova, M. Marnauza, M. Baitimirova, and D. Erts are with the Institute of Chemical Physics, University of Latvia, Riga LV1050, Latvia (e-mail: jana.andzane@lu.lv; krisjanis.buks@lu.lv; malvine.strakova@fizmati.lv; mikelis.marnauza@gmail.com; margarita.baitimirova@lu.lv; donats.erts@lu.lv).

M. Zubkins is with the Institute of Solid-State Physics, University of Latvia, Riga LV1063, Latvia (e-mail: zubkins@cfi.lu.lv).

M. Bechelany is with the European Institute of Membranes, University of Montpellier, CNRS, ENSCM, Place Eugene Bataillon, Montpellier 34095, France (e-mail: mikhael.bechelany@umontpellier.fr).

Digital Object Identifier 10.1109/TNANO.2019.2939862

1536-125X © 2019 IEEE. Personal use is permitted, but republication/redistribution requires IEEE permission.
See http://www.ieee.org/publications_standards/publications/rights/index.html for more information.

of the thin films occurred without carrier gas flow except for obtaining of disordered $Bi_2Se_3$ thin films on graphene surface.

Planar thin films on mica and graphene, disordered thin films on quartz/glass were obtained under the following deposition parameters: process pressure ∼2–3 Torr, substrate temperature 330–380 °C, no carrier gas flow.

Disordered thin films on CVD graphene can be obtained under the same deposition parameters, but with temporary gas flow (dynamic pressure 50–150 Torr) which was introduced into the furnace tube during the cooling process in the temperature interval 535–475 °C.

Typical thicknesses of the deposited thin films were 100–200 nm. Thickness of the thin films depends on the deposition time and amount of the source material. For the controlled doping of thin films, the dopant material was placed upstream from the source material. Depending on the required dopant concentration in the thin film, the temperature zones for the dopant placement varied between 460 and 585 °C.

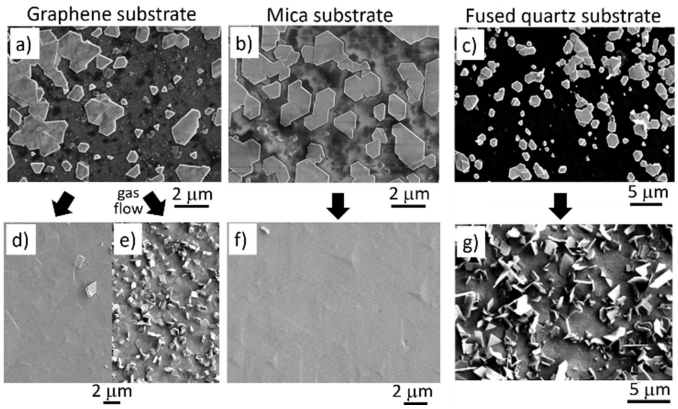


Fig. 1. a-b) SEM images of heteroepitaxial partially merged $Bi_2Se_3$ nanoplates on graphene (a) and mica (b) surfaces; c) SEM image of $Bi_2Se_3$ nuclei on glass surface; d-f) SEM images of planar (d – on graphene, f – on mica) and mixed (e – on graphene, g – on glass) continuous nanostructured $Bi_2Se_3$ thin films.

### *B. Investigation Methods*

Morphology, thickness, structure and composition of the $Bi_2Se_3$ nanoplates formed during the initial stage of the deposition and nanostructured thin films were inspected using field emission scanning electron microscope (SEM) Hitachi S-4800 equipped with an energy-dispersive X-ray (EDX) analyser Bruker XFLASH 5010, atomic force microscope (AFM) Asylum Research MFP-3D and X-ray diffraction spectroscopy (XRD) using powder diffractometer X'PERT MRD with Cu K$\alpha$ radiation source.

Transport properties of the thin films were measured using Hall effect measurement system HMS-5000 at room temperature and in the temperature range 90–300 K. Due to the technical reasons, transport properties of part of the samples were not characterized.

Thermoelectrical measurements were carried at room temperature (300 K) under ambient conditions using home-made device calibrated by Standard Reference Material 3451 for low temperature Seebeck coefficient (NIST). This device consisted of two Peltier elements, temperature control unit, HP multimeter 34401A and software for automatic data recording. For the in-plane measurements, the substrate with deposited thin film was placed over two Peltier elements held at constant temperatures 295 and 320 K respectively. Electrical contacts to the thin films were established using gold-plated spring-pins. The distance between the electrodes was 0.7–1 cm. The temperatures of the "hot" and "cold" sides of the thin film were determined using thermocouples placed on its surface using thermally conductive paste. Additionally, Seebeck coefficient and electrical conductivity of one of the planar $Bi_2Se_3$ thin films deposited on mica substrate was measured using thermal transport option of physical property measurement system (PPMS, DynaCool9T, Quantum Design).

## III. Results and Discussion

Morphology of the nanostructured thin films deposited by catalyst-free vapour-solid technique is governed by the properties of the substrate surface [11], [12]. At the beginning of the deposition process, the natural diffusion of the evaporated source material from the hot centre of the furnace tube results in random nucleation and further growth of $Bi_2Se_3$ nanoplates on the substrate surface, which corresponds to Vollmer-Weber (island) growth mode (Fig. 1a-c). Due to the intrinsically anisotropic bonding nature, the most energetically favourable orientation of $Bi_2Se_3$ nuclei is Q-layers parallel to the substrate surface. In the absence of any obstacles, the further lateral growth of the $Bi_2Se_3$ nuclei occurs symmetrically and faster than vertical due to the diffusion of adatoms to the edges of the nanoplates over its Se-passivated top surface [13]. For the substrates with low number of surface defects such growth results in formation of planar thin films. The use of the substrates with higher number of surface defects results in formation of disordered thin films.

### *A. Planar Not-Doped Thin Films*

The ideal substrates for obtaining of planar thin films are freshly cleaved mica and annealed graphene [12]. Mica can be easily cleaved along the (001) crystallographic planes. This provides atomically flat surface with very little number of chemical defects (dangling bonds). Its trapezohedral crystal structure with lattice constant a_o (s) = 5.19 Å has lattice mismatch with $Bi_2Se_3$ (a_o (s) = 4.14 Å) of ∼20%. Such lattice mismatch results in the Van der Waals epitaxy of the $Bi_2Se_3$ on mica surface [13]. In turn, monolayer graphene is a perfect substrate for the epitaxial $Bi_2Se_3$ growth due to the very small (<3%) $Bi_2Se_3$/graphene lattice mismatch [14]. The nanoplates formed on these substrates during the initial stage of the deposition (Fig. 1a,b) further coalesce together, thus forming continuous planar thin film (Fig. 1d,f).

Planar thin films cannot be obtained on fused quartz or glass substrates. The influence of the chemical surface defects (dangling bonds) or mechanical defects (asperities) induce randomly oriented growth of the nanoplates [11], [15], [16]. The dangling bonds originating from the defects on quartz/glass surface are introducing defects in the crystalline structure of growing nanoplates, thus promoting formation of other phases of $Bi_2Se_3$ crystals and changing growth direction of the nanoplates.

The preliminary passivation of the quartz/glass via annealing in Se atmosphere or annealing in $Ar/H_2$ atmosphere did not result in deposition of planar thin films. This indicates that mechanical irregularities on the substrate surface, promoting nanoplates growth under random angles relative to the substrate basis, may play significant role in formation of non-planar thin films.

### *B. Disordered Not-Doped Thin Films*

Deposition of the disordered $Bi_2Se_3$ thin films on quartz or glass surface (Fig. 1g) occurred under the same synthesis parameters as were used for the obtaining of planar thin films on mica and graphene surfaces. However, obtaining of the disordered thin films on the substrates promoting heteroepitaxial growth of $Bi_2Se_3$ nanostructures (mica, graphene) is very challenging. There were no synthesis parameters found to promote disordered $Bi_2Se_3$ growth on mica surface. Presumably, the artificial surface defects should be introduced to the mica surface to obtain disordered thin films. In turn, the disordered $Bi_2Se_3$ growth on the CVD graphene substrates can be achieved by the introduction of the temporary carrier gas flow during the $Bi_2Se_3$ deposition (as described in the Experimental section). As it is known, the CVD graphene has domain structure. The lateral growth of the heteroepitaxial $Bi_2Se_3$ nanoplates is hampered by the domain boundaries [10], [12]. Presumably, the temporary carrier gas flow, introduced in the furnace tube during the cooling process, causes rapid increase of vaporized source material concentration in the deposition area, thus promoting formation of oriented under different angles nanoplates at the edges of the heteroepitaxial $Bi_2Se_3$ nanoplates hampered by the graphene domain boundaries [10], [12]. Such growth results in formation of continuous nanostructured $Bi_2Se_3$ thin film consisting of mix of planar as well as oriented under different angles relative to the substrate surface nanoplates (Fig. 1e).

### *C. Structural Properties of Not-Doped $Bi_2Se_3$ Thin Films*

The percentage of Bi and Se found in the thin films corresponds to the stoichiometric $Bi_2Se_3$ (40% Bi: 60% Se). For the XRD investigation, diffraction peaks of the XRD patterns obtained for the planar and disordered $Bi_2Se_3$ thin films (Fig. 2a) can be indexed to the rhombohedral structure with cell units of a = b = 4.139 Å and c = 28.636 Å ([17], ref. code 00-033-0124). The XRD diffraction patterns of all $Bi_2Se_3$ thin films have highly intensive (*0 0 l*) peaks, as well as the (015) peak of very low intensity (Fig. 2b). With an exception of (015) peak, the affiliation of all presented in the XRD patterns diffraction peaks to a group (*0 0 3n*) indicates nearly pure growth of the thin films in single-crystalline phase with c-axis oriented perpendicularly to the substrate (planar growth).

Closer look at the XRD patterns (Fig. 2b) shows that the intensity of (015) diffraction peak for the planar $Bi_2Se_3$ thin film deposited on graphene substrate is negligible. The intensity of this peak slightly raises for the disordered thin film deposited on graphene substrates and becomes noticeable for the disordered $Bi_2Se_3$ thin film deposited on quartz substrate. This corresponds to the SEM images of the disordered thin films (Fig. 1e,g), showing higher proportion of the randomly oriented relative to the substrate surface nanoplates per unit area for the thin film deposited on quartz substrate in comparison with the graphene substrate. At the same time, the intensity of the (015) peak for the disordered $Bi_2Se_3$ thin film deposited on quartz is still very low in comparison with other peaks belonging to the (*0 0 3n*) group. This may indicate that the disordered nanoplates are formed only in the top layer of the thin film.

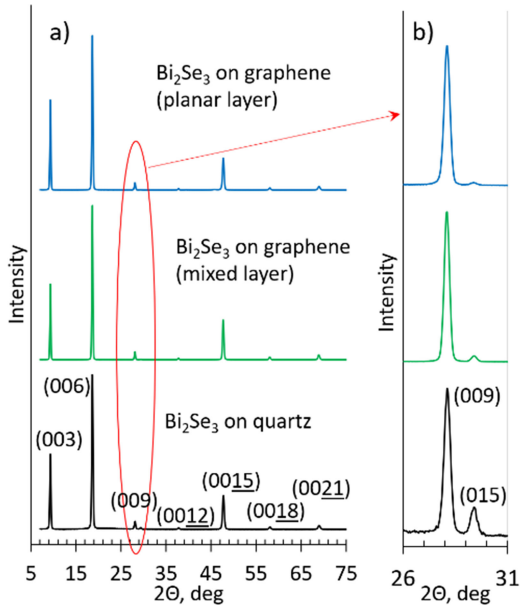


Fig. 2. a,b) Comparison between the XRD patterns of continuous nanostructured $Bi_2Se_3$ thin films deposited on quartz and graphene substrates.

TABLE I
ELECTRICAL TRANSPORT AND THERMOELECTRIC PROPERTIES OF CONTINUOUS NANOSTRUCTURED $Bi_2Se_3$ THIN FILMS DEPOSITED ON DIFFERENT SUBSTRATE AND MEASURED AT 300 K UNDER AMBIENT CONDITIONS

| No. | Substrate | Charge carrier conc., $cm^{-3}$ | Charge carrier mobility, $cm^2/(V{\cdot}s)$ | Conductivity, S/cm | Seebeck coeff., μV/K | Power factor, $\mu W/(cm{\cdot}K^2)$ |
|---|---|---|---|---|---|---|
| 1d | Quartz /glass | $2.2{\cdot}10^{18}$ | 510 | 180 | -182 | 6 |
| 2d | | $3.3{\cdot}10^{18}$ | 427 | 231 | -122 | 3.45 |
| 3d | | $4.7{\cdot}10^{18}$ | 356 | 271 | -74 | 1.45 |
| 4d | | $1.95{\cdot}10^{18}$ | 279 | 87 | -143 | 1.75 |
| 5p | Mica | $3.9{\cdot}10^{18}$ | 339 | 211 | -209 | 9.2 |
| 6p | | $2.35{\cdot}10^{18}$ | 453 | 171 | -162 | 4.5 |
| **7p** | | $\mathbf{2.9{\cdot}10^{18}}$ | **441** | **207** | **-227** | **10.7** |
| 8p | Graphene | $3.6{\cdot}10^{19}$ | 500 | 287 | 33 | 0.3 |
| 9p | | $4.2{\cdot}10^{18}$ | 257 | 172 | 89 | 1.35 |
| 10p | | $2{\cdot}10^{19}$ | 110 | 352 | 48 | 0.8 |
| 11p | | $1.3{\cdot}10^{19}$ | 148 | 556 | 36 | 0.73 |
| 12p | | $1.25{\cdot}10^{19}$ | 360 | 723 | 18 | 0.23 |

d-disordered thin films, p-planar thin films.

### *D. Electron Transport and Thermoelectrical Properties of Not-Doped $Bi_2Se_3$ Thin Films*

Experimental data for all characterized samples is summarized in Table I.

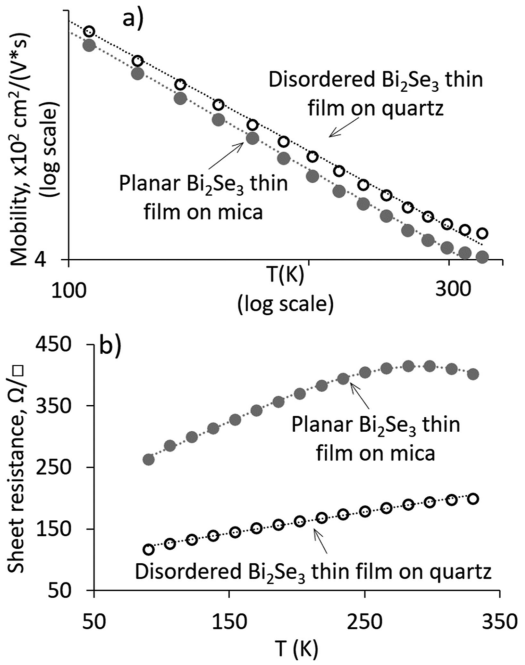


Fig. 3. Temperature dependence of the a) charge carrier mobility and b) sheet resistance of planar (grey circles) and disordered (hollow circles) $Bi_2Se_3$ thin films.

*1) $Bi_2Se_3$ Thin Films Deposited on Quartz/Glass and Mica Substrates:* Negative values of Seebeck coefficient shown by disordered thin films deposited on quartz/glass substrates and planar thin films deposited on mica substrates indicate domination of n-type conductivity in these films. Generally, the n-type conductivity in $Bi_2Se_3$ is determined by the native defects such as $Se_{Bi}$ antisites and/or Se vacancies, acting as active n-type dopants [18]. Charge carrier concentrations in these thin films were in the range from $\sim 2 \cdot 10^{18}$ up to $4.7 \cdot 10^{18} cm^{-3}$ with mobilities varying between 120 and 510 $cm^2/(V \cdot s)$. Presumably, such scatter of the experimental results origins from the different concentration of defects in the thin films. The highest mobility values showed by planar thin films deposited on mica ($\sim$450 $cm^2/(V \cdot s)$, sample No. 6p, Table I) and disordered (425–510 $cm^2/(V \cdot s)$, samples No. 1d and 2d, Table I) thin films are close to the values (320–1000 $cm^2/(V \cdot s)$) reported for the $Bi_2Se_3$ nanostructures with the low level (in order of $10^{13}$ $cm^{-2}$) of native charged impurity disorder in the thin film [19].

The temperature dependence of charge carrier mobilities for planar and disordered $Bi_2Se_3$ thin films with low level of native doping, deposited respectively on mica and quartz substrates (Table I, samples No. 2d and 6p), are shown in log-log scale in Fig. 3a. It has a power law scaling ($\sim T^n$) with exponents $n \approx -0.42$ and $-0.45$ for the disordered and planar thin films respectively. These exponents suggest that for the temperatures $\geq$100 K two scattering processes in these thin films may occur: electron-phonon ($\sim T^{-3/2}$) scattering and scattering on interfacial charged defects ($\sim T^{3/2}$), which may act as selective filter of low-energy minority charge carriers, thus improving the TE efficiency of the thin films [20].

The temperature dependence of the sheet resistance showed metallic behaviour for disordered $Bi_2Se_3$ thin film, while the planar $Bi_2Se_3$ thin film demonstrated a hump with a maximum around 280 K (Fig. 3b). This may indicate that planar $Bi_2Se_3$ thin films have multiband transport, which is typical for topological insulator nanostructures with low levels of native doping by Se vacancies [11].

Lower than 400 $cm^2/(V \cdot s)$ values of charge carrier mobilities (and relatively high charge carrier concentrations) of some of the disordered thin films deposited quartz/glass and planar thin films deposited on mica may be related to the higher concentration of charge impurities and defects in these thin films: lower charge carrier mobility and at the same time higher charge carrier concentration (Table I, samples No. 3d and 5p) may be related to positively charged defects in the grain boundaries ($Se_{Bi}$ antisites/Se vacancies), known to increase charge carrier concentration by producing of excess electrons; the lower carrier concentrations and at the same time lower mobility of the disordered thin film deposited on quartz (Table I, sample 4d) may be addressed to an increased concentration of defects (charge impurities on the grain boundaries, vacancies) due to the formed during the deposition discontinuities in this thin film.

The average absolute values of a Seebeck coefficient at room temperature for $Bi_2Se_3$ thin films were respectively 130 $\mu$V/K for the disordered thin films deposited on quartz/glass substrates (Table I, samples 1d–4d) and 200 $\mu$V/K for the planar thin films (Table I, samples 5p–7p).

These values exceed the absolute values of Seebeck coefficient reported for $Bi_2Se_3$ nanostructures synthesized via solvothermal method (115 $\mu$V/K) [21] and $Bi_2Se_3$ thin films with thickness 30 nm grown by molecular beam epitaxy (104.3 $\mu$V/K) [22], and are 2–3 times higher than the absolute value of the Seebeck coefficient of the bulk $Bi_2Se_3$ at room temperature (59 $\mu$V/K) [23]. Probably, the high values of Seebeck coefficient can be explained by the nanostructured nature of the $Bi_2Se_3$ thin films. Deposited thin films consist of coalesced nanoplates (Fig. 1) and thus have polycrystalline structure. It has been shown that the Seebeck coefficient of the polycrystalline materials depends on the size of the grain size and sharply increases when the length of grains is below 2 $\mu$m [25].

For the disordered $Bi_2Se_3$ thin films deposited on quartz/glass substrates, the Seebeck coefficient decreases with an increase of the charge carrier concentration (Table I, samples No. 1d–4d), which is consistent with the classic behaviour of Seebeck coefficient for bulk thermoelectric materials [25]. However, for the planar $Bi_2Se_3$ thin films deposited on mica substrates the value of Seebeck coefficient is not clearly related to the charge carrier concentration. Probably, this effect may be related the contribution of topological insulator surface states to the thermoelectrical transport [26] of the planar $Bi_2Se_3$ thin films.

The power factors calculated for the disordered $Bi_2Se_3$ thin films with low native doping level, obtained on quartz/glass were 3.45–6 $\mu W/cm \cdot K^2$ (Table I, samples No. 1d and 2d). Planar $Bi_2Se_3$ thin films obtained on mica showed power factor values up to 10.7 $\mu W/cm \cdot K^2$ at 300 K, which is close and even higher than the power factors reported for the MBE grown $Bi_2Se_3$ thin

films (up to 6 $\mu$W/cm·K$^2$) and pulsed laser deposition (up to 5.54 $\mu$W/cm·K$^2$) methods [27]. Presumably, the high power factors may be result of contribution of nanostructured nature and topological surface states in planar $Bi_2Se_3$ thin films. Power factors of the disordered $Bi_2Se_3$ thin films with higher number of defects (1.45–1.75 $\mu$W/cm·K$^2$, Table I, samples 3d and 4d) are comparable with the power factors reported for $Bi_2Se_3$ thin films grown by chemical solution (1–1.5 $\mu$W/cm·K$^2$).

*2) Planar $Bi_2Se_3$ Thin Films Deposited on Graphene Substrates:* $Bi_2Se_3$ thin films deposited on graphene substrates showed positive Seebeck coefficient, indicating p-type conductivity. Determined charge carrier concentrations in the planar $Bi_2Se_3$ thin films deposited on graphene ($4.2\cdot10^{18}$ – $3.6\cdot10^{19}$ cm$^{-3}$) were significantly higher in comparison with the thin films deposited on mica and quartz/glass substrates.

Presumably, the dominating charge carrier transport in graphene/$Bi_2Se_3$ system occurs through the graphene substrate due to its very low electrical resistance. In this case, the p-type conductivity and higher charge carrier concentrations may be related to the properties of the graphene substrates with some impact from the $Bi_2Se_3$ thin film, because the electrical contacts were placed on the surface of $Bi_2Se_3$ thin films and had no direct contact with the graphene substrates.

The charge carrier mobilities of these samples varied between 110 and 500 cm$^2$/(V·s) (Table I, samples 8p–12p), which is comparable with the charge carrier mobilities of $Bi_2Se_3$ thin films obtained on quartz/glass and mica substrates.

In-plane measurements of the Seebeck coefficient of the $Bi_2Se_3$ thin films deposited on graphene showed Seebeck coefficients values spread in the range 18–89 $\mu$V/K (avg. 45 $\mu$V/K). Considering that Seebeck coefficient of monolayer CVD graphene has been reported to be ~30 $\mu$V/K [28], it can be concluded that the result of in-plane measurements of the Seebeck coefficient $Bi_2Se_3$ layer on the graphene surface is most likely the combination of thermoelectric properties of graphene and thermoelectric effect given by the $Bi_2Se_3$ electrodes. Power factor of the $Bi_2Se_3$ thin films deposited on graphene were spread in the range (0.23–1.35 $\mu$W/cm·K$^2$) [29]. These results suggest that the graphene/$Bi_2Se_3$ systems are not suitable for in-plane determination of the thermoelectrical properties of $Bi_2Se_3$ thin films deposited on graphene. However, it should be noted that the thermoelectric properties of the $Bi_2Se_3$ thin films obtained on graphene are expected to be similar to the properties of planar $Bi_2Se_3$ thin films deposited on mica due to the similar deposition conditions and resulting structure of the thin films. The potential application of planar and disordered $Bi_2Se_3$ thin films on graphene substrates is through-plane thermoelectric devices, where graphene substrates will serve as top and bottom electrodes [10].

### *E. Thermoelectric Properties of Sb, Sn and Fe Doped Planar $Bi_2Se_3$ Thin Films Deposited on Mica Substrates*

As it is shown in the previous section, the planar $Bi_2Se_3$ thin films deposited on mica substrates exhibited the best thermoelectric performance. Such thin films were chosen for the further improvement of their thermoelectric properties by doping with Sb, Sn and Fe in different concentrations.

TABLE II
ELECTRICAL TRANSPORT AND THERMOELECTRIC PROPERTIES OF DOPED PLANAR $Bi_2Se_3$ THIN FILMS DEPOSITED ON MICA SUBSTRATES AND MEASURED AT 300 K UNDER AMBIENT CONDITIONS

| No. | Dopant | Dopant conc.% | Charge carrier conc., cm$^{-3}$ | Charge carrier mobility, cm$^2$/(V·s) | Conductivity, S/cm | Seebeck coeff., μV/K | Power factor, μW/(cm·K$^2$) |
|---|---|---|---|---|---|---|---|
| 1 | Sb | 1.5 | $1.44\cdot10^{19}$ | 590 | 1413 | -240 | 82.3 |
| 2 | | 3.5 | $1.86\cdot10^{18}$ | 41 | 368 | -206 | 1.7 |
| 3 | | 5 | $1.82\cdot10^{18}$ | 183 | 53.5 | -173 | 1.6 |
| 4 | Sn | 3 | - | 217 | 115 | -294 | 9.9 |
| 5 | | 8 | $6.3\cdot10^{18}$ | 306 | 330 | -170 | 9.5 |
| 6 | | 11 | $2.87\cdot10^{18}$ | 56 | 26 | -179 | 0.82 |
| 7 | Fe | 1 | $2.73\cdot10^{18}$ | 884 | 376 | -340 | 43.5 |
| 8 | | 2 | $2\cdot10^{18}$ | 907 | 286 | -320 | 29.3 |
| *9* | *Ref. 1* | *Non-doped* | *$2.9\cdot10^{18}$* | *441* | *207* | *-227* | *10.7* |
| *10* | *Ref. 2* | *Non-doped* | - | - | *502* | *-155* | *12.1* |

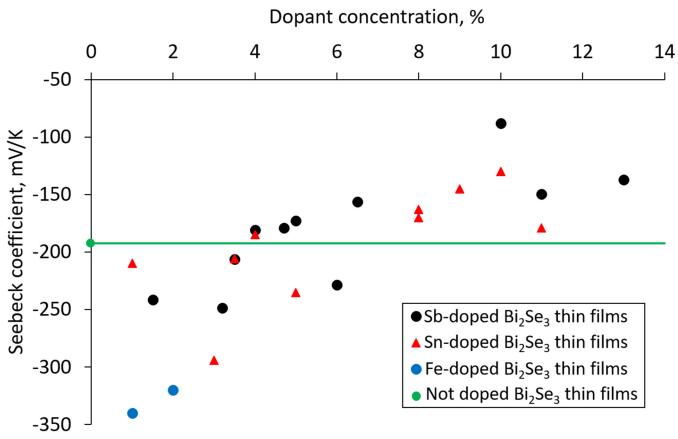


Fig. 4. Seebeck coefficient of Sb (black circles), Sn (red triangles) and Fe (blue squares) doped planar $Bi_2Se_3$ thin films as function of dopant concentration in these films. Green circle and green line represent the average value of the Seebeck coefficient of the non-doped reference samples.

Experimental data for doped thin films that have gone through the full range of measurements (charge carrier concentration and mobility, electrical conductivity, Seebeck coefficient) are summarized in Table II.

Fig. 4 shows the Seebeck coefficients of doped $Bi_2Se_3$ thin films as function of dopant concentration. Green line illustrates the average value of the Seebeck coefficients of two non-doped planar $Bi_2Se_3$ thin films deposited on mica and characterised with two different techniques (home-made device for thermoelectrical measurements (Table II, Ref. 1) and thermal transport measurements performed using Physical Property Measurement System (Table II, Ref. 2).

*1) Planar Thin Films Doped With Sb and Sn:* As it can be seen from the Fig. 4, the Seebeck coefficients of thin films

doped with Sb and Sn show similar dependence on the dopant concentration. The Seebeck coefficients slightly increase at the dopant concentrations of approx. 1–3% and tend to decrease with the further increase of dopant concentration. The absolute values of maximal Seebeck coefficient determined for the Sb- and Sn-doped thin films are respectively 248 $\mu$V/K for Sb concentration of 3.2%, and 294 $\mu$V/K for Sn dopant concentration of 3%. Despite the similar dependences of the Seebeck coefficient of $Bi_2Se_3$ thin films on Sb and Sn dopant concentrations, the mechanisms of impact of these dopants most likely differ. Presumably, similarly to previously reported experiments [3], [4], the low concentrations of Sb dopant in the $Bi_2Se_3$ thin films (Table II, sample No. 1) supress the bulk conductivity of the $Bi_2Se_3$, simultaneously lowering the Fermi level close to the conduction band edge. This results in enhancement of contribution of the protected from scattering metallic surface states to the total electrical conductivity of the sample and dramatic increase of the power factor up to $\sim$80 $\mu$W/(cm·K$^2$). Further increase of Sb dopant concentration in the $Bi_2Se_3$ samples may result in metal-to-insulator transition due to incorporation of orthorhombic $Sb_2Se_3$ guest lattice structures into host $Bi_2Se_3$ rhombohedral lattice, resulting in excessive conductivity suppression and increased scattering of charge carriers [3] (Table II, samples No. 2 and 3). It should be noted that the low charge carrier mobility of the sample No. 2 may be related also to formation of micro-cracks in this thin film, formed during the sample preparation for the measurements.

For the doping with Sn, the 1–3% dopant concentration probably results in creation of the impurity resonant level (RL) close to the conductive band edge and Fermi level, as it was theoretically predicted previously [6]. Such RL may partly hybridize with the host electronic structure of $Bi_2Se_3$, resulting in local re-distribution of the electronic states around conduction band leading to an increase of Seebeck coefficient (Table II, sample No. 4). However, the resulting power factor of Sn-doped thin films does not exceed the power factors of the best non-doped planar $Bi_2Se_3$ thin films. For the larger Sn concentrations, the efficiency of the RL may be diminished due to the shift of the Fermi level from the optimal for hybridization with the RL position or broadening of the RL and smearing of the resonant states with an increase of impurity concentration.

*2) Planar Thin Films Doped With Fe:* Planar thin films doped with Fe showed significantly increased charge carrier mobility and Seebeck coefficient in comparison with non-doped planar thin films (Table II samples No. 7 and 8). Power factor of Fe-doped thin films was by factor 3-4 higher than for non-doped thin films. This effect may be due to the introduction of magnetic impurities into the lattice structure of $Bi_2Se_3$ by substitution of Bi atoms with Fe. Probably, the introduction of magnetic impurities may result in the opening of Dirac band gap and creation of the resonant impurity levels, impacting the thermoelectric response [7]. However, despite the significant number of the researches related to the influence of magnetic impurities on topological properties of $Bi_2Se_3$, there are very few studies devoted to the thermoelectrical properties of magnetically doped $Bi_2Se_3$ at room temperature. Further investigation of properties of Fe-doped $Bi_2Se_3$ thin films is required for understanding of underlying mechanisms resulting in an increase of power factor of these films.

To summarize, the presented in this work catalyst-free vapour-solid deposition technique allowed to obtain high-quality planar nanostructured $Bi_2Se_3$ thin films on mica and graphene substrates, as well as disordered nanostructured $Bi_2Se_3$ thin films on quartz/glass and graphene substrates. To obtain disordered $Bi_2Se_3$ thin films on graphene substrates, the temporary carrier gas flow must be introduced into the furnace tube during the cooling process. Between all obtained thin films, the planar thin films deposited on mica showed the best thermoelectrical performance. The thermoelectrical power factor of these thin films is comparable with the power factor of the thin films grown using MBE method. Doping of the planar $Bi_2Se_3$ thin films with Sb and Fe in concentrations below 2% resulted in significant increase of the power factor of these films. Doping with Sn in concentrations of $\sim$3% may result in improvement of Seebeck coefficient, however, the increase of the power factor of the Sn-doped thin films was insufficient due to the reduced electrical conductivity. Our further research is aimed to completely characterize electronic transport properties of the $Bi_2Se_3$ thin films at different dopant concentration levels for optimal dopant concentration determination.

## REFERENCES


[1] M. S. Dresselhaus *et al.*, "New directions for low-dimensional thermoelectric materials," *Adv. Mater.*, vol. 19, pp. 1043–1053, 2007.

[2] J. Andzane *et al.*, "Structure-determined thermoelectric properties of $Bi_2Se_3$ thin films deposited by vapour-solid technique," in *Proc. IEEE 18th Int. Conf. Nanotechnol.*, 2018, pp. 1–5.

[3] C. H. Lee *et al.*, "Metal-insulator transition in variably doped (Bi1-xSbx)$_2$Se$_3$ nanosheets," *Nanoscale*, vol. 5, pp. 4337–4343, 2013.

[4] S. S. Hong, J. J. Cha, D. Kong, and Y. Cui, "Ultra-low carrier concentration and surface dominant transport in Sb-doped $Bi_2Se_3$ topological insulator nanoribbons," *Nat. Commun.*, vol. 3, 2012, Art. no. 757.

[5] S. K. Kushwaha *et al.*, "Sn-doped $Bi_{1.1}Sb_{0.9}Te_2S$ bulk crystal topological insulator with excellent properties," *Nat. Commun.*, vol. 7, 2016, Art. no. 11456.

[6] B. Wiedlocha, "Resonant levels, vacancies, and doping in $Bi_2Te_3$, $Bi_2Te_2Se$, and $Bi_2Se_3$ tetradymites," *J. Electron. Mater.*, vol. 45, 2016, Art. no. 3515.

[7] M. Zhong, S. Li, H.-J. Duan, L.-B. Hu, M. Yang, and R.-Q. Wang, "Effect of impurity resonant states on optical and thermoelectric properties on the surface of a topological insulator," *Sci. Rep.*, vol. 7, 2017, Art. no. 3971.

[8] J. T. Mlack, A. Rahman, G. L. Johns, K. J. T. Livi, and N. Marković, "Substrate-independent catalyst-free synthesis of high-purity $Bi_2Se_3$ nanostructures," *Appl. Phys. Lett.*, vol. 102, 2013, Art. no. 193108.

[9] J. Kosmaca, J. Andzane, M. Baitimirova, F. Lombardi, and D. Erts, "Role of nanoelectromechanical switching in the operation of nanostructured $Bi_2Se_3$ interlayers between conductive electrodes," *ACS Appl. Mater. Interfaces*, vol. 8, 2016, Art. no. 12257.

[10] M. Baitimirova *et al.*, "Vapour-solid synthesis and enhanced thermoelectric properties of non-planar bismuth selenide nanoplates on graphene substrate," *J. Mater. Sci.*, vol. 51, no. 8224, 2016, Art. no. 20163.

[11] J. Andzane *et al.*, "Catalyst-free vapour–solid technique for deposition of $Bi_2Te_3$ and $Bi_2Se_3$ nanowires/nanobelts with topological insulator properties," *Nanoscale*, vol. 7, 2015, Art. no. 15935.

[12] J. Andzane *et al.*, "Effect of graphene substrate type on formation of $Bi_2Se_3$ nanoplates," *Sci. Rep.*, vol. 9, 2019, Art. no. 4791.

[13] A. Zhuang *et al.*, "Controlling the lateral and vertical dimensions of $Bi_2Se_3$ nanoplates via seeded growth," *Nano Res.*, vol. 8, 2015, Art. no. 246.

[14] Y. Min *et al.*, "Solution-based synthesis of anisotropic metal chalcogenide nanocrystals and their applications," *J. Mater. Chem. C.*, vol. 2, 2014, Art. no. 6222.

[15] S.-K. Jerng *et al.*, "Ordered growth of topological insulator $Bi_2Se_3$ thin films on dielectric amorphous $SiO_2$ by MBE," *Nanoscale*, vol. 5, 2013, Art. no. 10618.
[16] G. Kunakova *et al.*, "Surface structure promoted high-yield growth and magnetotransport properties of $Bi_2Se_3$ nanoribbons," Scientific Reports 9, 2019, doi: 10.1038/s41598-019-47547-0, Art. no. 11328.
[17] M. C. Morris *et al.*, "Standard X-ray Diffraction Powder Patterns. NBS Monograph 25 - Section 18 - Data for 58 Substances," U.S. Department of Commerce/National Bureau of Standards, Washington, DC 20234, p. 16, 1981.
[18] L. Xue *et al.*, "First-principles study of native point defects in $Bi_2Se_3$," *AIP Adv.*, vol. 3, 2013, Art. no. 052105.
[19] D. Kim *et al.*, "Surface conduction of topological Dirac electrons in bulk insulating $Bi_2Se_3$," *Nat. Phys.*, vol. 8, 2012, Art. no. 459.
[20] P. Puneet *et al.*, "Preferential scattering by interfacial charged defects for enhanced thermoelectric performance in few-layered n-type $Bi_2Te_3$," *Sci. Rep.*, vol. 3, 2013, Art. no. 3212.
[21] K. Kadel, L. Kumari, W. Z. Li, J. Y. Huang, and P. P. Provencio, "Synthesis and thermoelectric properties of $Bi_2Se_3$ nanostructures," *Nanoscale Res. Lett.*, vol. 6, 2011, Art. no. 57.
[22] M. Guo *et al.*, "Tuning thermoelectricity in a $Bi_2Se3$ topological insulator via varied film thickness," *New J. Phys.*, vol. 18, 2016, Art. no. 015008.
[23] J. Navratil *et al.*, "Conduction band splitting and transport properties of $Bi_2Se_3$," *J. Solid State Chem.*, vol. 177, 2004, Art. no. 1704.
[24] Y. W. Gao, Y. Z. He, and L. L. Zhu, "Impact of grain size on the Seebeck coefficient of bulk polycrystalline thermoelectric materials," *Chin. Sci. Bull.*, vol. 55, 2010, Art. no. 16.
[25] T. M. Tritt, in *Encyclopedia of Materials: Science and Technology*, 2nd ed. Amsterdam, The Netherlands: Elsevier, 2002, pp. 1–11.
[26] N. Xu, Y. Xu, and J. Zhu, "Topological insulators for thermoelectrics," *NPJ Quantum Mater.*, vol. 2, 2017, Art. no. 51.
[27] P. H. Le, C.-N. Liao, C. W. Luo, J.-Y. Lin, and J. Leu, "Thermoelectric properties of bismuth-selenide films with controlled morphology and texture grown using pulsed laser deposition," *Appl. Surf. Sci.*, vol. 285P, 2013, Art. no. 657.
[28] Z. Sun, S. Liufu, and L. Chen, "Synthesis and characterization of nanostructured bismuth selenide thin films," *Dalton Trans.*, vol. 39, 2010, Art. no. 10883.
[29] X. Li, J. Yin, J. Zhou, Q. Wang, and W. Guo, "Exceptional high Seebeck coefficient and gas-flow-induced voltage in multilayer graphene," *Appl. Phys. Lett.*, vol. 100, 2012, Art. no. 183108.

Authors' photographs and biographies not available at the time of publication.